Published in final edited form as:
Circ Arrhythm Electrophysiol. 2011 June 1; 4(3): 407–417. doi:10.1161/CIRCEP.109.934208.

A Novel Lead Configuration for Optimal Spatio-Temporal Detection of Intracardiac Repolarization Alternans

Eric H. Weiss, MS, **Faisal M. Merchant, MD**, **Andre d'Avila, MD, PhD**, **Lori Foley, BS**, **Vivek Y. Reddy, MD**, **Jagmeet P. Singh, MD, PhD**, **Theofanie Mela, MD**, **Jeremy N. Ruskin, MD**, and **Antonis A. Armoundas, PhD**
Harvard-MIT Division of Health Sciences and Technology, Massachusetts Institute of Technology, Cambridge, MA (EHW, AAA) and the Massachusetts General Hospital, Division of Cardiology, Harvard Medical School, Boston, MA (ALdA, FM, VYR, LF, JS, TM, JNR, AAA)

Abstract

Background—Electrical alternans is a pattern of variation in the shape of electrocardiographic waveform that occurs every other beat. In humans, alternation in ventricular repolarization, known as repolarization alternans (RA), has been associated with increased vulnerability to ventricular tachycardia/fibrillation and sudden cardiac death.

Methods and Results—This study investigates the spatio-temporal variability of intracardiac RA and its relationship to body surface RA in an acute myocardial ischemia model in swine. We developed a real-time multi-channel repolarization signal acquisition, display and analysis system to record electrocardiographic signals from catheters in the right ventricle, coronary sinus, left ventricle, and epicardial surface prior to and following circumflex coronary artery balloon occlusion. We found that RA is detectable within 4 minutes following the onset ischemia, and is most prominently seen during the first half of the repolarization interval. Ischemia-induced RA was detectable on unipolar and bipolar leads (both in near- and far-field configurations) and on body surface leads. Far-field bipolar intracardiac leads were more sensitive for RA detection than body surface leads, with the probability of body surface RA detection increasing as the number of intracardiac leads detecting RA increased, approaching 100% when at least three intracardiac leads detected RA. We developed a novel, clinically-applicable intracardiac lead system based on a triangular arrangement of leads spanning the right ventricular (RV) and coronary sinus (CS) catheters which provided the highest sensitivity for intracardiac RA detection when compared to any other far-field bipolar sensing configurations ($p < 0.0001$).

Conclusions—In conclusion, intracardiac alternans, a complex spatio-temporal phenomenon associated with arrhythmia susceptibility and sudden cardiac death, can be reliably detected through a novel triangular RV-CS lead configuration.

Keywords

Arrhythmias; clinical electrophysiology; signal processing; intracardiac; alternans

Correspondence: Antonis A. Armoundas, PhD, Cardiovascular Research Center, Massachusetts General Hospitals, 149 13th Street, Charlestown, MA 02129, TEL: 617-726-0930, FAX: 617-726-5806, aarmoundas@partners.org.

Conflict of Interest Disclosures: TM **receives honoraria from** Medtronic < $10K**,** Biotronik < $10K**,** St Jude < $10K**. Dr. Mela also consults for** Biotronik < $ 10K. JNR has received research grants from Biosense Webster > $10K, St. Jude Medical > $10K. He has ownership interest in Cameron Health > $10K and InnerPulse > $10K. He works as a consultant for Medtronic > $10K and Biosense Webster < $10K. Additionally, he has received fellowship grants from Medtronic > $10K, St Jude > $10K and Boston Scientific > $10K

Introduction

Repolarization alternans (RA) reflects oscillations in cardiac repolarization that occur on an every-other-beat basis and can be visualized on the body surface electrocardiogram (ECG) as two distinct, alternating ST-segment and/or T-wave morphologies [1–3]. The presence of RA has been associated with an increased risk of sudden cardiac death (SCD) in patients with diverse pathophysiological conditions, including: (i) symptoms suggestive of ventricular arrhythmias [4–6], (ii) congestive heart failure or ejection fraction (EF) ≤ 40% [7, 8], and (iii) recent myocardial infarction (MI) [8–10].

Numerous experimental [11–17] and computational [18–20] studies have demonstrated that spatially heterogeneous action potential duration (APD) alternans can provide the substrate for re-entrant arrhythmias including ventricular tachycardia/ventricular fibrillation (VT/VF). Furthermore, functional spatial dispersion of refractoriness is also likely to contribute to the onset of VT/VF [11, 16, 21–27]. Therefore, it is conceivable that spatially localized cardiac RA leads to increased dispersion of refractoriness, wavefront fractionation, re-entry and VT/VF. Building on this paradigm, it is likely that the heart either passes through a stage of heightened RA on the way to VT/VF or RA occurs in tight conjunction with the onset of VT/VF [8].

Previous studies have demonstrated that RA is inducible *in vivo* by coronary artery occlusion,[28–30] and that RA is detectable from intracardiac electrograms [31–35]; however, intracardiac RA detection studies have been limited to spontaneously occurring or pacing-induced RA detected only by a right ventricular catheter [31–34] or the combination of right ventricular and coronary sinus catheters.[35]

The close association between RA and malignant arrhythmias raises the yet unconfirmed possibility that dynamic control of RA *in vivo* may prevent the onset of VT/VF. However, the first step in the attempt of modulating RA is the accurate detection of the complex spatio-temporal nature of RA from an intracardiac lead configuration. This study investigates the hypothesis that a minimum-order intracardiac lead configuration may be developed to accurately estimate the presence of intracardiac RA. We probed this hypothesis in a swine acute myocardial ischemia model, in which intracardiac RA and body surface RA were estimated from electrograms obtained from catheters placed in the right ventricle, coronary sinus, left ventricle, and left ventricular epicardium (trans-pericardial). To test this hypothesis, we characterized the fidelity of body surface and intracardiac electrogram recordings both prior to and following ischemia induction; we investigated the spatio-temporal effects of acute myocardial ischemia on body surface and intracardiac RA; we investigated the effects of intracardiac sensing vector on RA estimation; and we determined the most sensitive intracardiac lead combination for RA estimation.

Methods

Animal Preparation

Ten male Yorkshire swine (40–45 kg) were anesthetized and acutely instrumented in the Animal Electrophysiology Laboratory of the Massachusetts General Hospital. The protocol was approved by the Hospital's Animal Care and Use Committee.

Anesthesia was induced with Telazol (4.4 mg/kg) im and Xylazine (2.2 mg/kg) im. Each animal was intubated and placed on a mechanical ventilator, and anesthesia was maintained with Isoflurane (1.5–5%).

Percutaneous intracardiac access was achieved in the jugular veins and femoral arteries and veins using standard Seldinger technique [36, 37]. Decapolar catheters were placed under fluoroscopic guidance in the (i) right ventricle (RV), the distal lead being at the RV apex, (ii) coronary sinus (CS), the distal lead being at the distal CS, (iii) left ventricle (LV), the proximal lead being at the LV apex, and in five swine in the (iv) epicardial space (EPI). Pericardial access was obtained using a standard percutaneous subxiphoid approach as previously described [38]. An inferior vena cava catheter was inserted as a reference electrode for unipolar signals. An arterial line was used to monitor arterial blood pressure.

Standard electrocardiographic electrodes were placed on the animal's limbs and chest; the epidermis was excised at point of contact to maximize signal quality.

Regional myocardial ischemia was induced via balloon occlusion of the proximal left circumflex coronary artery utilizing standard percutaneous cardiac catheterization techniques.

Equipment and Data Collection Methods

Intracardiac and body surface (leads II and V4) electrocardiographic signals as well as arterial blood pressure were recorded through a Prucka Cardiolab (General Electric) electrophysiology system that provided 16 high fidelity analog output signals. The Prucka system provided front-end signal conditioning as well as isolation protection of the signal analysis system from defibrillation. Intracardiac signals were band-pass filtered 0.05–500 Hz, with 60 Hz notch filter and gain 250 V/V, and body surface signals were band-pass filtered 0.05–100 Hz, with 60 Hz notch filter and gain 2500 V/V.

We developed a real-time signal acquisition, analysis and display system for use in this study, consisting of custom software written in LabView 8.5 (National Instruments, Austin, TX) and MATLAB 7.6 (Mathworks, Natick, MA). This system supports the acquisition and display of all 16 Prucka output signals, sampled at 1000 Hz by a multi-channel 16-bit data acquisition card (National Instruments M-Series PCI6255), and supports the real-time analysis and display of a single selected signal. Data analysis software written in MATLAB was compiled and deployed into the real-time LabView data acquisition system.

Repolarization alternans estimates were obtained from the two body surface leads, 12 intracardiac unipolar leads (three in each of the right-ventricular, left-ventricular, epicardial and coronary sinus catheters), 4 far-field intra-catheter bipolar leads (one per catheter, derived by subtracting non-adjacent pairs of unipolar leads with 2.7–3.6 cm spacing), 4 near-field bipolar leads (one per catheter, derived by subtracting adjacent pairs of unipolar leads with 0.3 cm spacing), and 3 bipolar leads spanning the heart in a triangular configuration, formed between RV lead 1, CS lead 1, and CS lead 7: RV1CS1, RV1CS7, and CS7CS1.

Intracardiac and Body Surface Electrocardiographic Data Analysis

We modified a previously described alternans analysis algorithm [6, 31, 39] for the estimation of intracardiac RA in the current study.

We obtained preliminary R-wave time-points by applying a software-based QRS detection algorithm to surface electrogram lead V4. Preliminary QRS detections were refined and abnormal beats, e.g. premature ventricular complexes (PVCs) and aberrantly conducted beats, were identified using a template-matching QRS algorithm [39].

Briefly, for each new beat, an 80 ms window centered at the peak of the QRS complex was formed from the preliminary beat detection; an isoelectric PR segment was automatically

subtracted as a zero amplitude reference point (by estimating the mean voltage in a 10 ms window preceding the start of each QRS complex). A median QRS template was generated from all ‘normal’ QRS complexes across the previous 127 beats and the beat was aligned to the QRS template using cross-correlation. Cross-correlation was repeated twice for each new QRS complex to ensure proper QRS alignment. A beat was considered ‘abnormal’ if its correlation coefficient was less than a threshold value of 0.95 or if the preceding R-to-R (RR) interval was at least 10% shorter than the mean RR interval of the previous 7 beats.

Our beat classification decision matrix is presented in Table 1. Every time a beat was identified that did not meet the RR interval criterion (e.g. premature ventricular complex), the current, preceding, and subsequent beats were all labeled ‘abnormal’. When only the correlation criterion was not met (e.g. aberrant beat), only the current beat was labeled ‘abnormal’.

Once all abnormal beats were identified in a 128 beat sequence, each abnormal beat was substituted with a median odd or even template beat on a lead-by-lead basis (derived from the odd or even ‘normal’ beats respectively in the 128 beat sequence), depending on whether the abnormal beat was an even or odd beat.

Repolarization Interval Boundary Detection

Repolarization interval boundaries for RA analysis were independently determined for each of the body surface leads, intracardiac unipolar leads, and intracardiac bipolar leads to account for variability in the morphology as well as the timing of the T-wave between leads.

For each beat, initial T-wave boundaries were established using a rate-based T-wave window formula, in which the window begins 100 ms after the R-wave if the previous RR interval was greater than 770 ms, 7.8% of the RR interval plus 40 ms if the RR interval was between 320 and 770 ms, and 65 ms if the RR interval was less than 320 ms. The T-wave window ends 500 ms after the R-wave if the previous RR interval was greater than 770 ms, or at 65% of the RR interval if the previous RR interval was shorter than 770 ms.

T-wave boundaries were detected on a lead-by-lead basis by performing linear baseline adjustment across the T-wave window (using the approximate T-wave boundaries described above), squaring the T-wave, integrating the T-wave power, and determining new and more accurate T-wave boundaries at timings corresponding to 1% and 99% of the signal power, respectively.

QRS boundaries were detected using the above method, using an initial window extending from 50 ms prior to the QRS peak to either 80 ms after the QRS peak or to the beginning of the T-wave, whichever was shorter.

The repolarization interval was calculated as the end of the QRS complex to the end of the T-wave. Boundaries between the ST segment and T-wave were not calculated due to significant ST segment elevations during acute coronary artery occlusion

Repolarization Alternans Estimation

Spectral alternans estimation was performed on a beat-by-beat basis for each 128-beat data sequence using a 512-point power spectrum to improve the sampling resolution of the spectrum. To account for the spatial variability of RA, spectral estimation was independently performed for each lead.

Repolarization alternans indices were estimated as follows:

$$\text{alternans voltage } (\mu\text{V}) = \sqrt{\text{alternans peak} - \mu_{\text{noise}}}$$
$$K_{\text{score}} = \frac{\text{alternans peak} - \mu_{\text{noise}}}{\sigma_{\text{noise}}}$$

where the alternans peak is the peak in the aggregate power spectrum corresponding to 0.5 cycles/beat and the mean (μ_{noise}) and the standard deviation (σ_{noise}) of spectral noise are estimated from a predefined aggregate power spectrum noise window (0.43–0.46 cycles/beat). The alternans voltage is a direct measure of the presence of RA, while the alternans K_{score} is a measure of the statistical significance of the alternans voltage.

For each lead, RA was estimated on a beat-by-beat basis using a rolling 128-beat window that was shifted one beat at a time.

Estimation of Intracardiac Repolarization Alternans Thresholds

RA estimated from body surface electrograms in humans is deemed "positive" when both of the following criteria are met: (i) $K_{score} \geq 3$, and (ii) alternans voltage ≥ 1.0 μV [40]. To adjust the alternans voltage threshold to a level suitable for the anesthetized swine, we scaled the human alternans voltage threshold by the ratio of the mass of the average 40 kg swine heart, 177 g [41], to the mass of the average human heart, 320 g (0.55). We accordingly implemented a swine body surface alternans voltage threshold of 0.55 μV.

Because intracardiac unipolar and bipolar signals are larger in amplitude than the body surface signals, it was also necessary to proportionately scale the intracardiac alternans voltage thresholds to account for these greater amplitudes. Failure to scale the voltage thresholds in this manner would have led to increased sensitivity but reduced specificity for RA detection when comparing intracardiac to body surface leads, thereby introducing bias into the study.

Therefore, we devised a method in which we determined an intracardiac alternans voltage threshold on an animal-by-animal basis by first calculating an amplitude scale factor for each intracardiac lead, and then scaling the body surface alternans voltage threshold by this scale factor. Briefly, for each catheter lead, the signal amplitude was calculated as the square root of the mean signal power between 1 and 50 Hz. The amplitude scale factor for each lead was then calculated as the ratio of the mean signal amplitude, divided by the mean signal amplitude of all body surface leads. The alternans voltage threshold for each catheter was then calculated as the amplitude scale factor multiplied by the body surface threshold of 0.55 μV. The alternans voltage thresholds are displayed in the Online Supplement.

Positive RA was determined to be present on a given lead within a 128-beat analysis segment when the K_{score} exceeded an amplitude of 3 and the alternans voltage exceeded the alternans voltage threshold as estimated for that lead. If fewer than 90% of the beats within the analysis window were 'normal' beats (as defined above), the data segment was labeled indeterminate. [40]

To allow comparisons between recordings with unequal duration, we devised the index "alternans percent"; this index is calculated as the total number of positive RA sequences divided by the total number of positive and negative sequences, where each segment was classified positive if at least one lead on each catheter, or at least one body surface lead, indicated positive RA.

Clinical Data Collection Protocol

After all intracardiac catheters were positioned under fluoroscopic guidance, a single baseline dataset was recorded prior to circumflex coronary artery catheterization. An additional dataset was recorded immediately following coronary artery catheterization and balloon inflation.

Data Analysis

We evaluated the presence of RA at baseline and immediately following circumflex coronary artery balloon occlusion in all intracardiac and body surface leads for all 128-beat sequences with a good beat percentage exceeding 90%.

To explore the onset of RA during acute ischemia, we measured the time from the onset of circumflex balloon occlusion until RA was detected on each catheter, quantified as the time at which a minimum of 30 128-beat sequences were positive for RA.

To explore the temporal characteristics of ischemia-induced RA, we evaluated the alternans voltage and K_{score} throughout the repolarization interval (which extends from the beginning of the ST segment to the end of the T wave) for all intracardiac and body surface leads, and compared the difference in alternans voltage and K_{score} between the first and second half of the repolarization interval.

To explore the sensitivity of intracardiac RA estimation in relation to body surface RA estimation, we aggregated all post-occlusion 128-beat sequences from all study subjects and compared the proportion of RA-positive sequences as a function of the sensing configuration.

Statistical Analysis

Variables aggregated across all study subjects were expressed as mean of means ± standard deviation of means. The number of beats, record length, and mean heart rate in each dataset were compared before and after coronary artery occlusion using the Wilcoxon matched pairs signed rank test. The percentage of PVCs and percentage of indeterminate sequences in each dataset were compared before and after coronary artery occlusion by employing a generalized linear model with repeated measurements, and fitting this model using a generalized estimating equation (GEE) method.

Alternans voltage, K_{score}, and alternans percent were compared before and after coronary artery occlusion and across catheters using two-way ANOVA with repeated measurements; multiple comparisons utilized Tukey's HSD Test. RA onset time was compared across catheters using one-way ANOVA. Alternans voltage and K_{score} were compared across the first and second half of the repolarization interval and across catheters using two-way ANOVA with repeated measurements. Comparisons between proportions of RA-positive beats utilized a GEE method with repeated measurements. Comparisons between intracardiac leads and the RV-CS triangular lead configuration utilized the modified Obuchowski test (MO) for comparison of correlated proportions for clustered data.[42]

Statistical significance was determined by p-values < 0.05. Statistical analysis was performed using R (R: A Language and Environment for Statistical Computing, Vienna, Austria) and SAS (SAS Institute Inc, Cary, NC).

Results

Intracardiac and Body Surface Electrograms

Figure 1A shows representative examples of body surface and unipolar intracardiac electrograms obtained prior to coronary artery balloon inflation. These electrogams demonstrate that all catheter leads provide low-noise, high-fidelity, artifact-free signals, suitable for RA analysis. As is apparent in Figure 1A, the amplitude of unipolar intracardiac electrograms is larger than body surface electrograms. Across all study subjects, the average QRS amplitude was 0.53 ± 0.14 mV for body surface leads and 4.17 ± 1.99 mV for right ventricular, 1.86 ± 0.74 mV for coronary sinus, 4.40 ± 2.09 mV for left ventricular, and 4.44 ± 1.59 mV for epicardial unipolar catheter leads.

Because of the variability in T-wave morphology and timing among leads, repolarization interval boundaries were automatically and independently detected for each lead. Figure 1B shows not-to-scale examples of body surface and unipolar intracardiac electrograms demonstrating that repolarization interval boundaries are accurately delineated for further RA analysis, and that these boundaries vary significantly on a lead-by-lead basis.

Acute Myocardial Ischemia Induction

An average of 980 ± 330 beats were recorded per animal at baseline, and an average of 1358 ± 690 beats were recorded per animal following balloon occlusion (p=0.322, signed rank=17, N=10). The mean baseline record length was 562 ± 177 sec, and the mean post-occlusion record length was 725 ± 397 sec (p=0.492, signed rank=20, N=10).

The mean heart rate at baseline was 105.3 ± 8.7 bpm, and following coronary artery balloon occlusion increased to 115.6 ± 13.3 bpm, (p=0.084, signed rank=10, N=10). ST-segment elevations were observed in all ten study subjects on multiple body surface and intracardiac leads following balloon occlusion (see Figure 2).

The average percentage of PVCs at baseline was 2.0%, and following coronary artery balloon occlusion was 2.7% (p=0.232, GEE method). The percent of indeterminate sequences at baseline was 11.4%, and following coronary artery balloon occlusion was 16.2% (p=0.278, GEE method).

Repolarization Alternans in the Presence of Acute Myocardial Ischemia

To investigate the effect of acute myocardial ischemia on RA, we evaluated the mean alternans voltage, K_{score}, and percentage of RA-positive sequences at baseline and following balloon occlusion across all study subjects for each of the body surface and RV, CS, LV and EPI catheters. The alternans voltage is reported in Figures 3A; K_{score} is reported in Figures 3B; and the percentage of positive alternans beats is reported in Figure 3C.

We observed that the alternans voltage, K_{score}, and alternans percent all increased following acute ischemia induction (alternans voltage: $p < 0.0001$, $F=37.297$, $df=1$; K_{score}: $p < 0.0001$, $F=20.078$, $df=1$, $N=45$; alternans percent: $p < 0.0001$, $F=105.481$, $df=1$, $N=45$; where, N is the total number of catheter comparisons: 10 each of the body surface, RV, CS, and LV catheters, and 5 EPI).

Onset of Repolarization Alternans during Acute Ischemia

Figure 4A illustrates the increase in alternans voltage and K_{score} for a single subject following the onset of acute ischemia. The body surface K_{score} is plotted following acute circumflex coronary artery occlusion at time 0. In this example, the alternans voltage and K_{score} increase significantly beginning 175 sec following occlusion.

In three out of the ten study subjects, RA was present immediately following balloon occlusion. These subjects were excluded from onset time analysis, as RA may have begun to develop prior to balloon occlusion, potentially on account of partial vessel occlusion during guiding catheter placement or balloon delivery. Figure 4B summarizes the compiled results from the other seven study subjects. The average alternans onset time was 190, 229, 191, 218, and 149 sec for body surface, RV, CS, LV, and EPI catheters, respectively. No statistically significant difference was observed as a function of catheter type, including between body surface and intracardiac catheters ($p=0.137$, $F=1.934$, $df=4$, $N=7$; where, N is the number of study subjects used in this comparison).

Temporal Characteristics of Repolarization Alternans

To explore the temporal characteristics of ischemia-induced RA, we normalized each repolarization interval to time-values between 0–100% (where 0% corresponds to the beginning of the ST segment and 100% to the end of the T wave), and calculated the average alternans voltage and K_{score} at each normalized time-value across all RA-positive repolarization sequences for each study subject.

Figure 5A presents the aggregate alternans voltage for each lead across the repolarization interval, averaged across all study subjects. The alternans voltage takes its maximum value at 31.4% ± 9.8% of the repolarization interval when averaged across all leads. Figure 5B presents the aggregate alternans K_{score} for each lead across the repolarization interval. The alternans K_{score} takes its maximum value at 29.0% ± 8.3% of the repolarization interval when averaged across all leads.

To compare the alternans voltage and K_{score} amplitudes in the first half versus the second half of the repolarization interval, the average alternans voltage and K_{score} for all RA-positive segments were first calculated across the first and second half of the repolarization interval for each study subject, then aggregated across all study subjects. Figure 5C shows a comparison of the mean alternans voltage in the first half (0–50%) of the repolarization interval (squares) versus the second half (50–100%) of the repolarization interval (circles). The alternans voltage is greater in the first half of the repolarization interval than the second half ($p=0.0007$, $F=12.501$, $df=1$, $N=39$; where, N is the total number of catheter comparisons with RA-positive segments). Figure 5D shows a comparison of the mean alternans K_{score} in the first half of the repolarization interval (squares) versus the second half (circles). The alternans K_{score} is greater in the first half of the repolarization interval than the second half ($p=0.0002$, $F=15.247$, $df=1$, $N=39$).

The Effect of Sensing Vector on Repolarization Alternans Estimation

Because unipolar electrograms integrate a large volume of cardiac tissue, they provide less spatial localization of cardiac events than bipolar electrograms; unipolar electrograms are also more susceptible to motion artifact than bipolar electrograms [43, 44].

To analyze the effect of the sensing lead configuration on RA detection, we compared RA estimates obtained from unipolar, far-field bipolar, and near-field bipolar lead configurations in each catheter following circumflex coronary artery balloon occlusion. Specifically, we estimated the (i) alternans voltage, (ii) K_{score}, and (iii) alternans percent, which we display in Figures 6A–C, respectively.

In Figure 6A, alternans voltage varies with sensing configuration ($p=0.007$, $F=5.219$, $df=2$, $N=35$, where N is the total number of catheter comparisons: 10 each of the RV, CS, and LV catheters, and 5 EPI). Alternans voltage estimated from both unipolar and far-field sensing configurations was significantly greater than when estimated from the near-field sensing configuration ($p=0.010$ and 0.031, respectively). In Figure 6B we see no statistical

difference in K_{score} as a function of sensing configuration (p=0.097, F=2.395, df=2, N=35). In Figure 6C, we see no difference in alternans percent as a function of sensing configuration (p=0.350, F=1.061, df=2, N=35).

Intracardiac versus Body Surface Alternans Estimation

Because the benefits of far-field intracardiac sensing include better spatial localization of sensing and less susceptibility to noise than unipolar sensing vectors, we hereafter employed far-field bipolar intracardiac leads for comparison to body surface RA. We employed four far-field intra-catheter bipolar leads - one per catheter - derived by subtracting non-adjacent pairs of unipolar leads with 2.7–3.6 cm spacing. We additionally employed a triangular lead configuration, consisting of leads RV1CS1, RV1CS7, and CS7CS1, for this analysis; each of these leads was found to be positive for RA in 52.5%, 48.4%, and 40.1% of all post-occlusion beat sequences, respectively (N=9639 beat sequences across all 10 study subjects).

Table 2 shows a 2×2 contingency table comparing the estimation of RA on body surface versus intracardiac leads for all post-occlusion beat sequences. 75.0% of beat sequences were positive for RA on at least one body surface lead, and 76.3% of beat sequences were positive for RA on at least one intracardiac lead. Furthermore, 90.3% of beat sequences positive for RA on a body surface lead were positive for RA on an intracardiac lead, and 88.7% of beat sequences positive for RA on an intracardiac lead were positive for RA on a body surface lead (p=0.691, χ_1^2=0.158, MO).

To address the question of whether RA detection using intracardiac leads improves the sensitivity of RA detection compared to body surface electrograms alone, we estimated the conditional probabilities of a positive body surface RA detection, given a positive far-field bipolar intracardiac RA detection for all beat sequences (N=9639). In Figure 7A, we plot the probability that a body surface lead is positive for RA given that a far-field bipolar intracardiac lead configuration is positive, from each of the RV, CS, LV, EPI, and triangular RV-CS lead configurations. The probability that a body surface lead is positive is 97.1% (CI: 90.4–99.2%, GEE) when an RV far-field bipolar lead is positive, 91.0% (CI: 79.3–96.4%, GEE) when a CS far-field bipolar lead is positive, 97.6% (CI: 93.4 - 99.1%, GEE) when an LV far-field bipolar lead is positive, 79.7% (CI: 58.3–96.1%, GEE) when an EPI far-field bipolar lead is positive, and 92.9% (CI: 84.7–96.8%, GEE) when a lead from a triangular RV-CS lead is positive.

In Figure 7B we plot the probability that a body surface lead is positive for RA given that a specified number of far-field bipolar intracardiac lead configurations is positive for RA (quantified across all beat sequences). We observe that the greater the number of far-field bipolar intracardiac lead configurations that is positive for RA, the greater the probability RA is seen on the body surface, approaching 100% when at least three intracardiac lead configurations detect RA.

To examine the sensitivity of intracardiac RA detection, in Figure 7C we plot the probability that a far-field bipolar intracardiac lead configuration is positive for RA, given that RA is seen on the body surface, for each of the RV, CS, LV, EPI, and triangular RV-CS lead configurations (quantified across all beat sequences). When a body surface lead is positive (N=7225), the probability that a triangular RV-CS lead is positive is 80.8%, greater than any other intracardiac lead configuration. The RV-CS positive percentage was significantly larger than for the CS configuration (p=0.006, χ_1^2=7.58, MO), and trended toward statistical significance for RV-CS vs. RV (p=0.090, χ_1^2=2.87, MO), RV-CS vs. LV (p=0.056, χ_1^2=3.64, MO), and RV-CS vs. EPI (p=0.154, χ_1^2=2.03, MO) comparisons.

In Figure 7D, we plot the probability that at least X far-field bipolar intracardiac lead configurations are positive for RA given that RA is positive in a body surface lead, where X = 1, 2, 3, 4, or all intracardiac leads. We see that when RA is detected on the body surface, at least one intracardiac lead also detects RA 90.3% of the time.

To examine which intracardiac lead combination is most sensitive for RA detection, in Figure 7E we plot the probability that a far-field bipolar intracardiac lead configuration is positive for RA, given that at least one intracardiac far-field lead is positive, for each of the RV, CS, LV, EPI, and triangular RV-CS far-field intracardiac lead configurations. When an intracardiac lead is positive (N=7358), the probability that a triangular RV-CS lead is positive is 85.5%, greater than any other intracardiac lead configuration. The RV-CS positive percentage was significantly larger than for the RV configuration (p=0.040, χ_1^2=4.23, MO), the CS configuration (p=0.004, χ_1^2=8.16, MO), and the LV configuration (p=0.035, χ_1^2=4.46, MO), but not for the EPI configuration (p=0.270, χ_1^2=1.22, MO).

Discussion

This study aims to investigate the hypothesis that the spatio-temporal nature of intracardiac RA may be captured through a minimum-order of intracardiac leads. To achieve this aim we have employed a swine acute myocardial ischemia model and have developed and utilized a system that is capable of acquiring up to 16 electrograms, from the body surface as well as catheters placed in the right ventricle, coronary sinus, left ventricle, and left ventricular epicardium, and estimating RA in real-time.

The present study is the first to provide a comprehensive and systematic approach into exploring the ability to record intracardiac RA in the presence of myocardial ischemia. Specifically, we have shown that *first*, in swine within 4 minutes following the onset of an ischemic episode, ischemia induces RA that can be detected by unipolar, near- and far-field bipolar intracardiac leads as well as leads on the body surface; *second*, during acute ischemia, RA is most prominently seen early in repolarization; *third*, far-field bipolar electrograms provide the preferred intracardiac lead configuration for the estimation of intracardiac RA; *fourth*, in the presence of body surface RA, at least one intracardiac far-field bipolar lead detects RA 90% of the time; *fifth*, the sensitivity for RA detection is improved by employing leads from multiple intracardiac catheters; and *sixth*, we demonstrate that a simple, clinically appropriate, intracardiac triangular RV-CS lead configuration provides the highest intracardiac sensitivity for estimating RA.

In light of the extensive pre-clinical [11, 13 , 14–16, 19] and clinical data [31–34] demonstrating an association between heightened RA and the onset of malignant arrhythmias including VT/VF, the accurate detection and potential modulation of RA may hold promise as a method to preempt VT/VF. Implantable cardioverter-defibrillators (ICDs) have demonstrated efficacy in secondary[45], and primary [46–48] prevention of SCD. However, a major drawback of current ICD therapy is the ability to terminate an arrhythmia only after the arrhythmia has started, thereby exposing patients to hemodynamic consequences such as loss of consciousness during arrhythmia and uncomfortable ICD shocks to terminate arrhythmia [49]. Therefore, although unproven, the ability to detect a potentially unstable arrhythmic substrate could result to delivery of therapy prior to the clinical onset of arrhythmia which could potentially be an attractive way to improve current ICD technology. Additionally, numerous studies have demonstrated a relationship between both appropriate and inappropriate ICD shocks and worse outcomes including heart failure progression and death [50]. Although patients with ICD shocks may have a more malignant underlying disease process, the possibility of a direct adverse impact from ICD shock therapy on long term outcomes remains a concerning possibility [51]. Therefore, developing strategies that would

predict the onset of a tachyarrhythmic event and deliver preemptive therapy, could potentially result to reduction of ICD shocks and improvement of outcomes.

We [31] and others [31–34,35] have previously shown that ICD-derived electrograms can be used to estimate the presence of RA prior to a tachyarrhythmic event. Building on those prior investigations, in this study, we have demonstrated in a systematic approach that far-field bipolar signals obtained from leads in the RV and CS is the optimal configuration for intracardiac RA detection and can be applied to future work for RA detection in ICD electrograms in humans. Therefore, our findings represent an important first step in testing the hypothesis that detection and modulation of RA may be capable of preempting malignant arrhythmias and preventing SCD.

While this study was not designed to provide localized RA estimates from near-field bipolar leads that are in close proximity to the area of ischemia/infarction, the dynamic nature of the electrophysiological properties near the core of an ischemic or infarcted territory makes it clinically impossible to always have a near-field bipolar lead in that area. Fortunately, our data suggest that far-field bipolar leads are superior to near-field bipolar leads in detecting RA during myocardial ischemia. Furthermore, the adoption of a novel intracardiac lead configuration consisting of bipolar leads between the RV and CS catheters provides a broader three-dimensional “view” of the myocardium and a wider solid angle to the heart when compared to near-field bipolar leads from intracardiac catheters. In light of currently available biventricular devices for cardiac resynchronization therapy, the application of a triangular RV-CS lead configuration is a potentially clinically feasible means to optimize intracardiac RA detection.

In conclusion, these results indicate that RA induced by left circumflex coronary artery occlusion in swine can be detected from intracardiac electrograms with improved spatial resolution compared to that obtained from body surface ECGs. These observations support the hypothesis that intracardiac alternans analysis is a viable alternative to surface ECG alternans analysis, and provides greater spatial sensitivity and specificity in the determination of potentially arrhythmogenic cardiac tissue.

Study Limitations

A limitation of this study is the lack of correlation between RA and arrhythmia susceptibility. Indeed the incidence of VT/VF in this study was not sufficient to generate receiver-operator curves for both intracardiac and body-surface signals. This has been the case because occlusion of the circumflex coronary artery was guided by the intent to induce RA without compromising the electrical stability of the animal.

Supplementary Material

Refer to Web version on PubMed Central for supplementary material.

Acknowledgments

This work was conducted with support from Harvard Catalyst | The Harvard Clinical and Translational Science Center (NIH Award #UL1 RR 025758 and financial contributions from Harvard University and its affiliated academic health care centers). The authors are grateful to Hui Zheng, PhD (Assistant Professor in Medicine, MGH Biostatistics Center, Harvard Medical School) for his expert advice with the statistical analysis of this manuscript.

Funding Sources: The work was supported by a Scientist Development Grant (#0635127N) and a Pre-doctoral Fellowship (#0815767D) from the American Heart Association, by NIA grant 1R21AG035128 and NIH grant 1RO1HL103961. This work was also supported by a Fellowship and a Science Award from the Center for Integration of Medicine and Innovative Technology (CIMIT), the Deane Institute for Integrative Research in Atrial Fibrillation and Stroke and the Cardiovascular Research Society.

References

1. Armoundas AA, Nanke T, Cohen RJ. Images in cardiovascular medicine. T-wave alternans preceding torsade de pointes ventricular tachycardia. Circulation. 2000; 101:2550. [PubMed: 10831532]
2. Puletti M, Curione M, Righetti G, Jacobellis G. Alternans of the ST segment and T wave in acute myocardial infarction. J Electrocardiol. 1980; 13:297–300. [PubMed: 7411001]
3. Salerno JA, Previtali M, Panciroli C, Klersy C, Chimienti M, Regazzi Bonora M, Marangoni E, Falcone C, Guasti L, Campana C, Rondanelli R. Ventricular arrhythmias during acute myocardial ischaemia in man. The role and significance of R-ST-T alternans and the prevention of ischaemic sudden death by medical treatment. Eur Heart J. 1986; 7 (Suppl A):63–75. [PubMed: 3720777]
4. Gold MR, Bloomfield DM, Anderson KP, El-Sherif NE, Wilber DJ, Groh WJ, Estes NA 3rd, Kaufman ES, Greenberg ML, Rosenbaum DS. A comparison of T-wave alternans, signal averaged electrocardiography and programmed ventricular stimulation for arrhythmia risk stratification. J Am Coll Cardiol. 2000; 36:2247–2253. [PubMed: 11127468]
5. Armoundas AA, Rosenbaum DS, Ruskin JN, Garan H, Cohen RJ. Prognostic significance of electrical alternans versus signal averaged electrocardiography in predicting the outcome of electrophysiological testing and arrhythmia-free survival. Heart. 1998; 80:251–256. [PubMed: 9875084]
6. Rosenbaum DS, Jackson LE, Smith JM, Garan H, Ruskin JN, Cohen RJ. Electrical alternans and vulnerability to ventricular arrhythmias. N Engl J Med. 1994; 330:235–241. [PubMed: 8272084]
7. Klingenheben T, Zabel M, D'Agostino RB, Cohen RJ, Hohnloser SH. Predictive value of T-wave alternans for arrhythmic events in patients with congestive heart failure. Lancet. 2000; 356:651–652. [PubMed: 10968440]
8. Armoundas AA, Hohnloser SH, Ikeda T, Cohen RJ. Can microvolt T-wave alternans testing reduce unnecessary defibrillator implantation? Nat Clin Pract Cardiovasc Med. 2005; 2:522–528. [PubMed: 16186850]
9. Armoundas AA, Tomaselli GF, Esperer HD. Pathophysiological basis and clinical application of T Wave alternans. JACC. 2002; 40:207–217. [PubMed: 12106921]
10. Ikeda T, Saito H, Tanno K, Shimizu H, Watanabe J, Ohnishi Y, Kasamaki Y, Ozawa Y. T-wave alternans as a predictor for sudden cardiac death after myocardial infarction. Am J Cardiol. 2002; 89:79–82. [PubMed: 11779531]
11. Pastore JM, Girouard SD, Laurita KR, Akar FG, Rosenbaum DS. Mechanism linking T-wave alternans to the genesis of cardiac fibrillation. Circulation. 1999; 99:1385–1394. [PubMed: 10077525]
12. Tachibana H, Kubota I, Yamaki M, Watanabe T, Tomoike H. Discordant S-T alternans contributes to formation of reentry: a possible mechanism of reperfusion arrhythmia. Am J Physiol. 1998; 275:H116–121. [PubMed: 9688903]
13. Shimizu W, Antzelevitch C. Cellular and ionic basis for T-wave alternans under long-QT conditions. Circulation. 1999; 99:1499–1507. [PubMed: 10086976]
14. Pastore JM, Rosenbaum DS. Role of structural barriers in the mechanism of alternans-induced reentry. Circ Res. 2000; 87:1157–1163. [PubMed: 11110773]
15. Baker LC, London B, Choi BR, Koren G, Salama G. Enhanced dispersion of repolarization and refractoriness in transgenic mouse hearts promotes reentrant ventricular tachycardia. Circ Res. 2000; 86:396–407. [PubMed: 10700444]
16. Choi BR, Salama G. Simultaneous maps of optical action potentials and calcium transients in guinea-pig hearts: mechanisms underlying concordant alternans. J Physiol. 2000; 529:171–188. [PubMed: 11080260]
17. Petkova-Kirova PS, Gursoy E, Mehdi H, McTiernan CF, London B, Salama G. Electrical remodeling of cardiac myocytes from mice with heart failure due to the overexpression of tumor necrosis factor-alpha. Am J Physiol Heart Circ Physiol. 2006; 290:H2098–2107. [PubMed: 16339842]
18. Fox JJ, Bodenschatz E, Gilmour RF Jr. Period-doubling instability and memory in cardiac tissue. Phys Rev Lett. 2002; 89:138101. [PubMed: 12225067]

19. Qu Z, Garfinkel A, Chen PS, Weiss JN. Mechanisms of discordant alternans and induction of reentry in simulated cardiac tissue. Circulation. 2000; 102:1664–1670. [PubMed: 11015345]
20. Watanabe MA, Fenton FH, Evans SJ, Hastings HM, Karma A. Mechanisms for discordant alternans. J Cardiovasc Electrophysiol. 2001; 12:196–206. [PubMed: 11232619]
21. Laurita KR, Girouard SD, Akar FG, Rosenbaum DS. Modulated dispersion explains changes in arrhythmia vulnerability during premature stimulation of the heart. Circulation. 1998; 98:2774–2780. [PubMed: 9851966]
22. Laurita KR, Girouard SD, Rudy Y, Rosenbaum DS. Role of passive electrical properties during action potential restitution in intact heart. Am J Physiol. 1997; 273:H1205–1214. [PubMed: 9321808]
23. Lee HC, Mohabir R, Smith N, Franz MR, Clusin WT. Effect of ischemia on calcium-dependent fluorescence transients in rabbit hearts containing indo 1. Correlation with monophasic action potentials and contraction. Circulation. 1988; 78:1047–1059. [PubMed: 2844438]
24. Qian YW, Clusin WT, Lin SF, Han J, Sung RJ. Spatial heterogeneity of calcium transient alternans during the early phase of myocardial ischemia in the blood-perfused rabbit heart. Circulation. 2001; 104:2082–2087. [PubMed: 11673350]
25. Wu Y, Clusin WT. Calcium transient alternans in blood-perfused ischemic hearts: observations with fluorescent indicator fura red. Am J Physiol. 1997; 273:H2161–2169. [PubMed: 9374749]
26. Chinushi M, Restivo M, Caref EB, El-Sherif N. Electrophysiological basis of arrhythmogenicity of QT/T alternans in the long-QT syndrome: tridimensional analysis of the kinetics of cardiac repolarization. Circ Res. 1998; 83:614–628. [PubMed: 9742057]
27. Chinushi M, Kozhevnikov D, Caref EB, Restivo M, El-Sherif N. Mechanism of discordant T wave alternans in the in vivo heart. J Cardiovasc Electrophysiol. 2003; 14:632–638. [PubMed: 12875425]
28. Qian YW, Sung RJ, Lin SF, Province R, Clusin WT. Spatial heterogeneity of action potential alternans during global ischemia in the rabbit heart. Am J Physiol Heart Circ Physiol. 2003; 285:H2722–2733. [PubMed: 12907420]
29. Carson DL, Cardinal R, Savard P, Vermeulen M. Characterisation of unipolar waveform alternation in acutely ischaemic porcine myocardium. Cardiovasc Res. 1986; 20:521–527. [PubMed: 3779749]
30. Konta T, Ikeda K, Yamaki M, Nakamura K, Honma K, Kubota I, Yasui S. Significance of discordant ST alternans in ventricular fibrillation. Circulation. 1990; 82:2185–2189. [PubMed: 2242541]
31. Armoundas AA, Albert CM, Cohen RJ, Mela T. Utility of Implantable Cardioverter Defibrillator Electrograms to Estimate Repolarization Alternans Preceding a Tachyarrhythmic Event. J Cardiovasc Electrophysiol. 2004; 15:594–597. [PubMed: 15149432]
32. Swerdlow CD, Zhou X, Voroshilovsky O, Abeyratne A, Gillberg J. High amplitude T-wave alternans precedes spontaneous ventricular tachycardia or fibrillation in ICD electrograms. Heart Rhythm. 2008; 5:670–676. [PubMed: 18452868]
33. Paz O, Zhou X, Gillberg J, Tseng HJ, Gang E, Swerdlow C. Detection of T-wave alternans using an implantable cardioverter-defibrillator. Heart Rhythm. 2006; 3:791–797. [PubMed: 16818208]
34. Christini DJ, Stein KM, Hao SC, Markowitz SM, Mittal S, Slotwiner DJ, Iwai S, Das MK, Lerman BB. Endocardial detection of repolarization alternans. IEEE Trans Biomed Eng. 2003; 50:855–862. [PubMed: 12848353]
35. Selvaraj RJ, Picton P, Nanthakumar K, Mak S, Chauhan VS. Endocardial and epicardial repolarization alternans in human cardiomyopathy: evidence for spatiotemporal heterogeneity and correlation with body surface T-wave alternans. J Am Coll Cardiol. 2007; 49:338–346. [PubMed: 17239715]
36. Schoenfeld MH, McGovern B, Garan H, Ruskin JN. Long-term reproducibility of responses to programmed cardiac stimulation in spontaneous ventricular tachyarrhythmias. Am J Cardiol. 1984; 54:564–568. [PubMed: 6475774]
37. Wilber DJ, Garan H, Ruskin JN. Electrophysiologic testing in survivors of cardiac arrest. Circulation. 1987; 75:III146–153. [PubMed: 3549048]

38. Sosa E, Scanavacca M, d'Avila A, Pilleggi F. A new technique to perform epicardial mapping in the electrophysiology laboratory. J Cardiovasc Electrophysiol. 1996; 7:531–536. [PubMed: 8743758]
39. Smith JM, Clancy EA, Valeri CR, Ruskin JN, Cohen RJ. Electrical alternans and cardiac electrical instability. Circulation. 1988; 77:110–121. [PubMed: 3335062]
40. Cambridge Heart CH. 2000 Operator's Manual. 2004.
41. Allan JS, Rose GA, Choo JK, Arn JS, Vesga L, Mawulawde K, Slisz JK, Allison K, Madsen JC. Morphometric analysis of miniature swine hearts as potential human xenografts. Xenotransplantation. 2001; 8:90–93. [PubMed: 11328578]
42. Yang Z, Sun X, Hardin JW. A note on the tests for clustered matched-pair binary data. Biometrical Journal. 2010; 52:638–652. [PubMed: 20976694]
43. DeCaprio V, Hurzeler P, Furman S. A comparison of unipolar and bipolar electrograms for cardiac pacemaker sensing. Circulation. 1977; 56:750–755. [PubMed: 912833]
44. Hauser RG. Bipolar Leads for Cardiac Pacing in the 1980s: A Reappraisal Provoked by Skeletal Muscle Interference. Pacing Clin Electrophysiol. 1982; 5:34–37. [PubMed: 6181471]
45. AVIDInvestigators. A comparison of antiarrhythmic-drug therapy with implantable defibrillators in patients resuscitated from near-fatal ventricular arrhythmias. N Engl J Med. 1997; 337:1576–1583. [PubMed: 9411221]
46. Moss AJ, Hall WJ, Cannom DS, Daubert JP, Higgins SL, Klein H, Levine JH, Saksena S, Waldo AL, Wilber D, Brown MW, Heo M. Improved survival with an implanted defibrillator in patients with coronary disease at high risk for ventricular arrhythmia. Multicenter Automatic Defibrillator Implantation Trial Investigators. N Engl J Med. 1996; 335:1933–1940. [PubMed: 8960472]
47. Moss AJ, Zareba W, Hall WJ, Klein H, Wilber DJ, Cannom DS, Daubert JP, Higgins SL, Brown MW, Andrews ML. Prophylactic implantation of a defibrillator in patients with myocardial infarction and reduced ejection fraction. N Engl J Med. 2002; 346:877–883. [PubMed: 11907286]
48. Buxton AE, Lee KL, DiCarlo L, Gold MR, Greer GS, Prystowsky EN, O'Toole MF, Tang A, Fisher JD, Coromilas J, Talajic M, Hafley G. Electrophysiologic testing to identify patients with coronary artery disease who are at risk for sudden death. Multicenter Unsustained Tachycardia Trial Investigators. N Engl J Med. 2000; 342:1937–1945. [PubMed: 10874061]
49. Stevenson WG, Stevenson LW. Prevention of Sudden Death in Heart Failure. J Cardiovasc Electrophysiol. 2001; 12:112–114. [PubMed: 11204073]
50. Cevik C, Perez-Verdia A, Nugent K. Implantable cardioverter defibrillators and their role in heart failure progression. Europace. 2009; 11:710–715. [PubMed: 19357142]
51. Tereshchenko LG, Faddis MN, Fetics BJ, Zelik KE, Efimov IR, Berger RD. Transient local injury current in right ventricular electrogram after implantable cardioverter-defibrillator shock predicts heart failure progression. J Am Coll Cardiol. 2009; 54:822–828. [PubMed: 19695461]

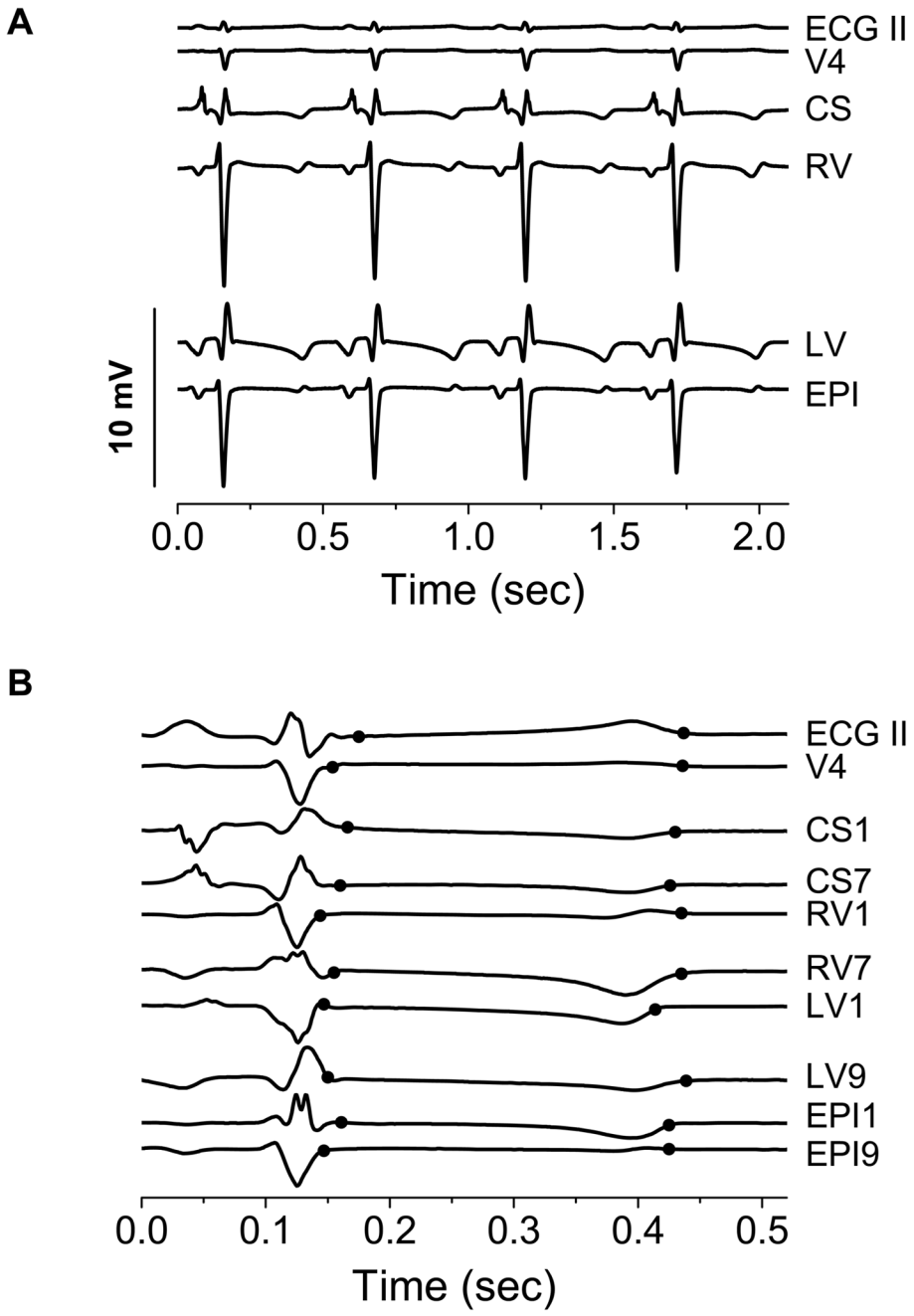

Figure 1.

Representative electrograms. (A) Electrograms from surface leads ECG II and V4 and unipolar intracardiac leads referenced to an electrode in the inferior vena cava. The amplitude of unipolar intracardiac electrograms is considerably larger than body surface electrograms. CS: Coronary Sinus, RV: Right Ventricular, LV: Left Ventricular, and EPI: Epicardial. (B) Electrograms illustrating the repolarization interval boundary determination method. The two black circles marking each lead correspond to repolarization interval begin and end points, respectively. These boundaries vary across leads because of the variability in T-wave morphology among leads. CSX: Coronary Sinus, RVX: Right Ventricular, LVX:

Left Ventricular, and EPIX: Epicardial, where X is the lead number along a decapolar catheter, 1 being most distal (signals not drawn to scale).

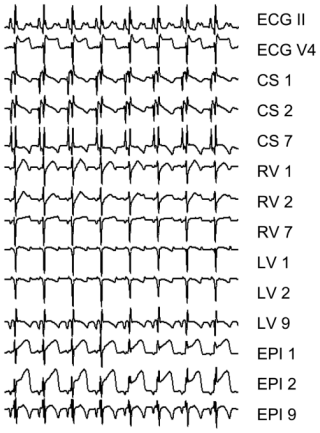

Figure 2.

Body surface ECGs and unipolar intracardiac electrograms post-circumflex coronary artery balloon occlusion. ST segment elevations are clearly visible on multiple electrograms. Repolarization alternans is also visible on multiple channels, including ECG V4 and RV 1. CSX: Coronary Sinus, RVX: Right Ventricular, LVX: Left Ventricular, and EPIX: Epicardial, where X is the lead number along a decapolar catheter, 1 being most distal (signals not drawn to scale).

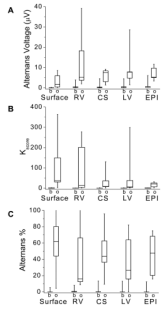

Figure 3.

Alternans voltage, K_{score}, and alternans percent at baseline (b) and immediately following circumflex coronary artery balloon occlusion (o) for body surface and RV, CS, LV and EPI unipolar intracardiac leads. Boxes define the 25%-median-75% data range, and vertical whiskers extend to the minimum and maximum. (A) Alternans voltage, (B) K_{score}, and (C) alternans percent. The alternans percent is equal to the total number of positive RA sequences divided by the total number of positive and negative sequences. Alternans voltage, K_{score}, and alternans percent all increased following acute ischemia induction, (ANOVA $p < 0.0001$, $F=37.297$, $df=1$, $N=45$; $p < 0.0001$, $F=20.078$, $df=1$, $N=45$; and $p < 0.0001$, $F=105.481$, $df=1$, $N=45$, respectively, where N represents the overall sample size).

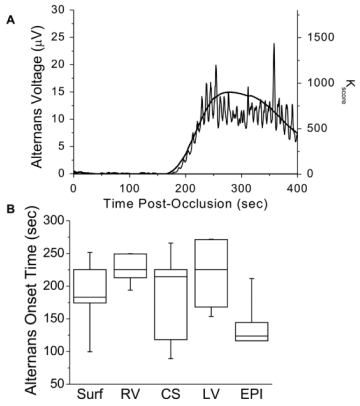

Figure 4.

Timing of alternans onset. (A) Alternans voltage and K_{score} following acute circumflex coronary artery balloon occlusion at time 0. The body surface alternans voltage (thin line) and K_{score} (thick line) are plotted for a single study subject; both alternans voltage and K_{score} significantly increase beginning 175 sec after balloon occlusion. (B) Alternans onset time across all study subjects for body surface and intracardiac catheters. Onset time for each catheter was determined as the time at which a minimum of 30 beats were positive for RA. Boxes define the 25%-median-75% data range, vertical whiskers extend to the min and max. No statistically significant difference was observed between body surface or intracardiac catheters (one-way ANOVA p=0.137, F=1.934, df=4, N=7, where N represents the overall sample size).

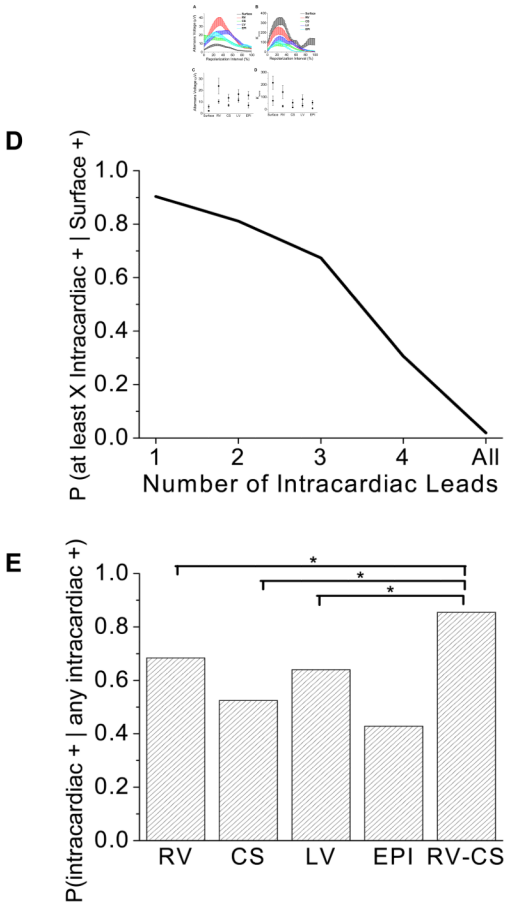

Figure 5.

Temporal characteristics of repolarization alternans during the repolarization interval, which extends from the beginning of the ST segment (0%) to the end of the T wave (100%). (A) Alternans voltage, plotted at each point in the repolarization interval, from 0% to 100%, for each of the body surface and unipolar RV, CS, LV, and EPI leads, compiled across all study subjects for all RA-positive segments. The alternans voltage takes its maximum at 31.4% ± 9.8% of the repolarization interval when averaged across all leads. (B) K_{score}, plotted as in (A). K_{score} takes its maximum at 29.0% ± 8.3% of the repolarization interval when averaged across all leads. For (A) and (B), error bars are s.e.m., shown only as positive deflections to improve data visualization. (C) Comparison of the mean alternans voltage in the first half (0–50%) of the repolarization interval (squares) versus the second half (50–100%) of the repolarization interval (circles). Error bars are s.e.m. The alternans voltage is greater in the first half of the repolarization interval than the second half (ANOVA p=0.0007, F=12.501, df=1, N=39, where N represents the overall sample size). (D) Comparison of the mean K_{score} in the first half of the repolarization interval (squares) versus the second half of the repolarization interval (circles). Error bars are s.e.m. K_{score} is greater in the first half of the repolarization interval than the second half (ANOVA p=0.0002, F=15.247, df=1, N=39).

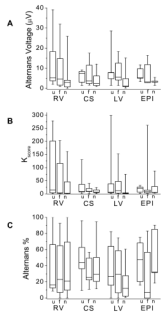

Figure 6.

Evaluation of unipolar (u), far-field bipolar (f), and near-field bipolar (n) intracardiac RA following circumflex coronary artery balloon occlusion for (A) alternans voltage, (B) K_{score}, and (C) alternans percent. Boxes define the 25%-median-75% data range, and vertical whiskers extend to the minimum and maximum. (A) Alternans voltage varies with sensing configuration (ANOVA p=0.007, F=5.219, df=2, N=35, where N represents the overall sample size). Unipolar and far-field bipolar alternans voltage were significantly greater than near-field (p=0.010 and 0.031, respectively). (B) No statistical difference in K_{score} was observed as a function of sensing configuration (ANOVA p=0.097, F=2.395, df=2, N=35). (C) No statistical difference in alternans percent was observed as a function of sensing configuration (p=0.350, F=1.061, df=2, N=35).

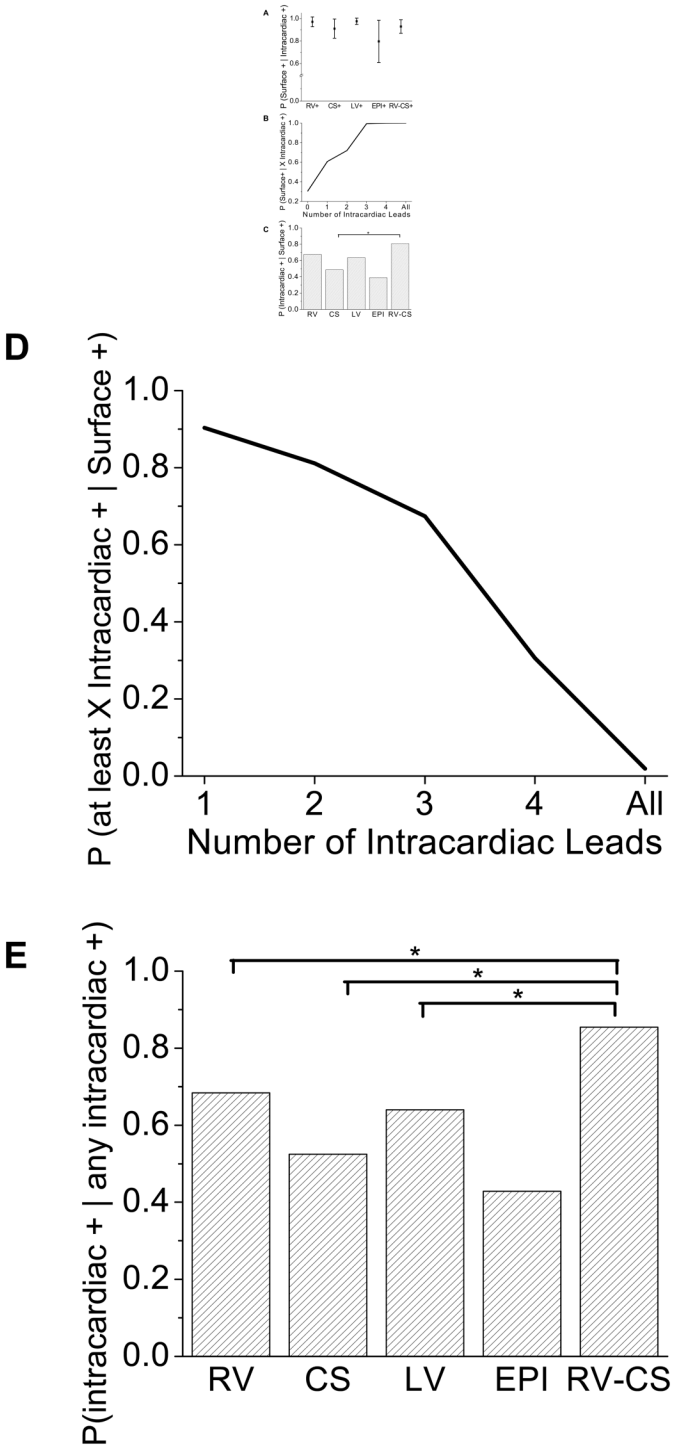

Figure 7.

Body surface versus intracardiac alternans detection. (A) Probability that a body surface lead is positive for RA given that the corresponding intracardiac lead is positive for RA, for each of the RV, CS, LV, EPI, and triangular RV-CS far-field intracardiac lead configurations. Error bars define 95% confidence intervals. (B) Probability that a body surface lead is positive for RA given a specified number of far-field intracardiac leads is positive for RA.

The greater the number of positive for RA far-field intracardiac lead configurations, the greater the probability that RA is seen on the body surface. (C) Probability that an intracardiac lead configuration is positive for RA given that RA is seen on the body surface, for each of the RV, CS, LV, EPI, and triangular RV-CS far-field intracardiac lead configurations (N=7225, overall sample size). The RV-CS positive percentage was significantly larger than for the CS configuration ($p=0.006$, $\chi_1^2=7.58$, MO), and trended toward statistical significance for RV-CS vs. RV ($p=0.090$, $\chi_1^2=2.87$, MO), RV-CS vs. LV ($p=0.056$, $\chi_1^2=3.64$, MO), and RV-CS vs. EPI ($p=0.154$, $\chi_1^2=2.03$, MO) comparisons. (D) Probability that at least X far-field intracardiac leads are positive for RA given that RA is seen on the body surface, where X = 1, 2, 3, 4, or all intracardiac leads. (E) Probability that a far-field bipolar intracardiac lead is positive for RA, given that at least one intracardiac far-field lead is positive for RA, for each of the RV, CS, LV, EPI, and triangular RV-CS far-field intracardiac lead configurations. The RV-CS positive percentage was significantly larger than for the RV configuration ($p=0.040$, $\chi_1^2=4.23$, MO), the CS configuration ($p=0.004$, $\chi_1^2=8.16$, MO), and the LV configuration ($p=0.035$, $\chi_1^2=4.46$, MO), but not for the EPI configuration ($p=0.270$, $\chi_1^2=1.22$, MO). Statistically significant comparisons are marked by an *.

Table 1

Decision matrix and justification for abnormal beat classification. Beats are labeled ‘abnormal’ based upon correlation and RR interval delta criteria. Correlations below 0.95 indicate a morphology non-match, and ΔRR interval less than −10% indicate an early beat. An abnormal beat is substituted with median even/odd template beat correspondingly prior to alternans analysis.

Case	Correlation Criterion	ΔRR Interval Criterion	Abnormal Beats	Justification
A	< 0.95	< −10%	3 beats: previous, present, next	*Premature Ventricular Contraction*
B	< 0.95	≥ −10%	1 beat: present	*Aberrantly conducted sinus beat (i.e. bundle branch block)*
C	≥ 0.95	< −10%	3 beats: previous, present, next	*Supraventricular*
D	≥ 0.95	≥ −10%	0	*Normal*

Table 2

2×2 contingency table comparing RA estimation on body surface versus intracardiac leads for all post-occlusion beat sequences aggregated across all study subjects. Intracardiac +: if at least one far-field bipolar lead (RV, CS, LV, EPI, or RV-CS) is positive for RA. Body surface +: if at least one body surface lead is positive for RA. 76.3% of beat sequences were positive for RA on at least one intracardiac lead and 75.0% of beat sequences were positive for RA on at least one body surface lead. Furthermore, 90.3% of beat sequences positive for RA on a body surface lead were positive for RA on an intracardiac lead, and 88.7% of beat sequences positive for RA on an intracardiac lead were positive for RA on a body surface lead ($p=0.691$, $\chi 12=0.158$, Modified Obuchowski).

		Body Surface	
		+	−
Intracardiac	+	6527 (67.7%)	831 (8.6%)
	−	698 (7.2%)	1583 (16.4%)